Available online at www.sciencedirect.com
ScienceDirect
Journal of Bionic Engineering 8 (2011) 1–9

Development of Air Vehicle with Active Flapping and Twisting of Wing

Sangyol Yoon[1], Lae-Hyong Kang[2], Sungho Jo[1]

1. *Department of Computer Science*, *Korea Advanced Institute of Science and Technology*, *Daejeon* 305-701, *Korea*
2. *Department of Aerospace Engineering*, *Korea Advanced Institute of Science and Technology*, *Daejeon* 305-701, *Korea*

Abstract

This paper addresses mechanisms for active flapping and twisting of robotic wings and assesses flying effectiveness as a function of twist angle. Unlike the flapping motion of bird wings, insects generally make a twisting motion at the root of their wings while flapping, which makes it possible for them to hover in midair. This work includes the development of a Voice Coil Motor (VCM) because a flapping-wing air vehicle should be assembled with a compact actuator to decrease size and weight. A linkage mechanism is proposed to transform the linear motion of the VCM into the flapping and twisting motions of wings. The assembled flapping-wing air vehicle, whose weight is 2.86 g, produces an average positive vertical force proportional to the twist angle. The force saturates because the twist angle is mechanically limited. This work demonstrates the possibility of developing a flapping-wing air vehicle that can hover in midair using a mechanism that actively twists the roots of wings during flapping.

Keywords: biomimetic, flapping-wing air vehicle, flapping, twisting, voice coil motor, linkage mechanism

Copyright © 2011, Jilin University. Published by Elsevier Limited and Science Press. All rights reserved.
doi: 10.1016/S1672-6529(11)60007-3

1 Introduction

Biomimetic engineering is an effective design approach because the forms and driving mechanisms of animals and insects are highly efficient and robust. For example, fish skin reduces skin friction or drag, and the running mechanisms of insects have been imitated in the development of robust six-legged running robots. Both birds and insects fly using a flapping motion of the wings. However, insects can also hover in midair, which is difficult for most birds.

In order to develop flying robots that mimic natural wing flapping motions, many researchers have designed flappers based on the motion of flying insects, which can be captured using a high speed camera. These flappers mimic the structure, dimensions, and weight of insect wings. Some insects, such as beetles, can fly by twisting the roots of their wings while flapping[1]; others, such as butterflies, fly by changing their body pitch angle while flapping[2].

The most significant flying robot was developed by Wood[3]. Its wings are actuated by PZT-5H, which is a soft piezoelectric crystal material and requires high voltage, and are twisted passively while flapping to obtain sufficient thrust. High voltage actuators might not be suitable for very small flying robots. To enable an active twisting motion, a mechanism for a flying robot with a linkage structure using PZT-5H was developed by Sitti[4]. The linkage structure was simple and small. However, it also had a high voltage requirement due to the PZT-5H. An alternative linkage structure, using geared DC motors, was developed by Żbikowski *et al*.[5], and McIntosh *et al*.[6]. Theses structures could be supplied with a low voltage due to the DC motors. However, the mechanism by Żbikowski *et al*. was complicated and consisted of many mechanical parts. Although the mechanism by McIntosh *et al*. was less complex than that by Żbikowski *et al*., its size and weight were larger (the wing span was 48 cm and the weight was 50 g).

In this work, two actuators made of Voice Coil Motors (VCM), which consist of moving coil and fixed magnet, are used to actively twist the roots of the robot wings, and to flap them. The VCM can be actuated with a standard battery and allows the robot size to be kept to a minimum. The mechanism to actively twist the wings can be used to help control the direction of flight.

Corresponding author: Sungho Jo
E-mail: shjo@cs.kaist.ac.kr

This paper addresses the design of a flying robot that can hover in midair. This robot includes a wing flapping mechanism and two actuators to drive the wings while the driving power is supplied externally. The effectiveness of the wing twisting mechanism is assessed.

2 Characteristics of flying insects

Flying insects are composed of wings to generate aerodynamic force, thorax muscles to flap the wings and a thorax to transmit muscular force to the wings. The transmission mechanism that drives the wings is one of the most important components of the flight system because this mechanism flaps the wings and twists the wings about their longitudinal axis to generate aerodynamic force and to control flight direction. The center of mass of the wing is located behind the longitudinal axis of the wing[7]. This causes the wings to twist about the longitudinal axis at the end of each stroke. The amount of twist increases as the distance from the axis to the center of mass of the wing increases.

The elastic thorax of insects can be characterized by the stiffness of the mechanical system. The resonant frequency of the elastic thorax is used as the flapping frequency to reduce power consumption during flight[8].

Insect wings consist of soft membranes and veins. Veins function as tubes for nerves and blood, and they also provide support to membranes while flapping and twisting the wings. In general, the veins are arranged so that the leading edge of the wing is more rigid than the trailing edge of the wing. This bends the camber of the wing in opposite direction for the upstroke and downstroke. However, this effect is not fully reversible[8]. The ratio of wing mass to body mass ranges from 0.5 to 4% in dipterans and hymenopterans[9].

When insects hover in midair by flapping their wings, air is accelerated downwards. The lifting force by the induced velocity must be in balance with the insect weight so that they can hover in midair[10], that is

$$W = 2\rho A_e v^2, \tag{1}$$

where W is the weight of insect, ρ is the density of air, A_e is the effective area of wing or sweeping area and v is the velocity induced by flapping. The velocity induced by flapping can be expressed as the flapping frequency, $\dot{\theta}_r$, and the effective length of wing, R_e. The effective length of wing is the distance from the root to the center of the wing area, because the distributed pressure of air can be considered as a resultant force acting on the center of the wing area. Typically, the center of the wing area is placed at $0.4R$ to $0.6R$, where R is the length of wing[9,11–13]. The effective area of the wing can be expressed by the wing area, A, the flapping stroke, θ_r, and the twist angle, θ_t. Therefore, Eq. (1) can be rewritten as

$$W = 2\rho A \cos\theta_r \cos\theta_t (R_e \dot{\theta}_r)^2. \tag{2}$$

3 Design of the flying robot

3.1 Structures for flapping and twisting

Flying insects generate lift using the flapping motion of their wings. However, the flapping motion alone cannot lift their body because the total force equals zero if the effective area of the wings at the upstroke is the same as at the downstroke. Therefore, it is essential to decrease the effective area of the wings on the upstroke while flapping. In this design, a mechanism using a ball-joint is adopted to twist wings while flapping, as shown in Fig. 1.

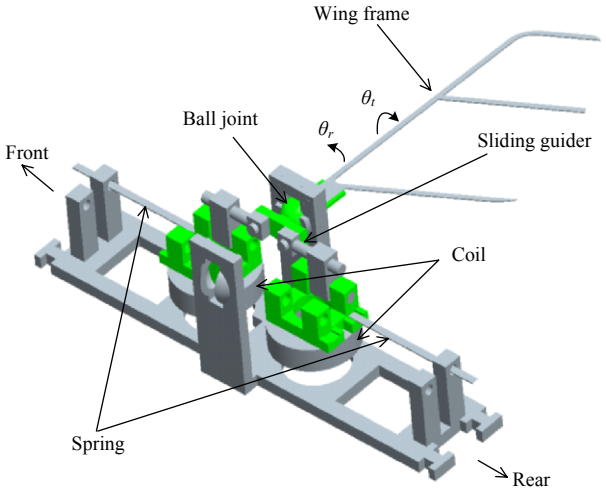

Fig. 1 An illustration of air vehicle described in this paper.

Two actuators are placed on the front and rear sides of the ball-joint, respectively. Wings can be flapped by moving two coils synchronously and twisted by moving them asynchronously - the front coil remains stationary and the other moves downwards at the beginning of the upstroke. Fig. 2 depicts the above procedure. The arrow shows the direction of actuator movement and the dot indicates that the coil remains stationary.

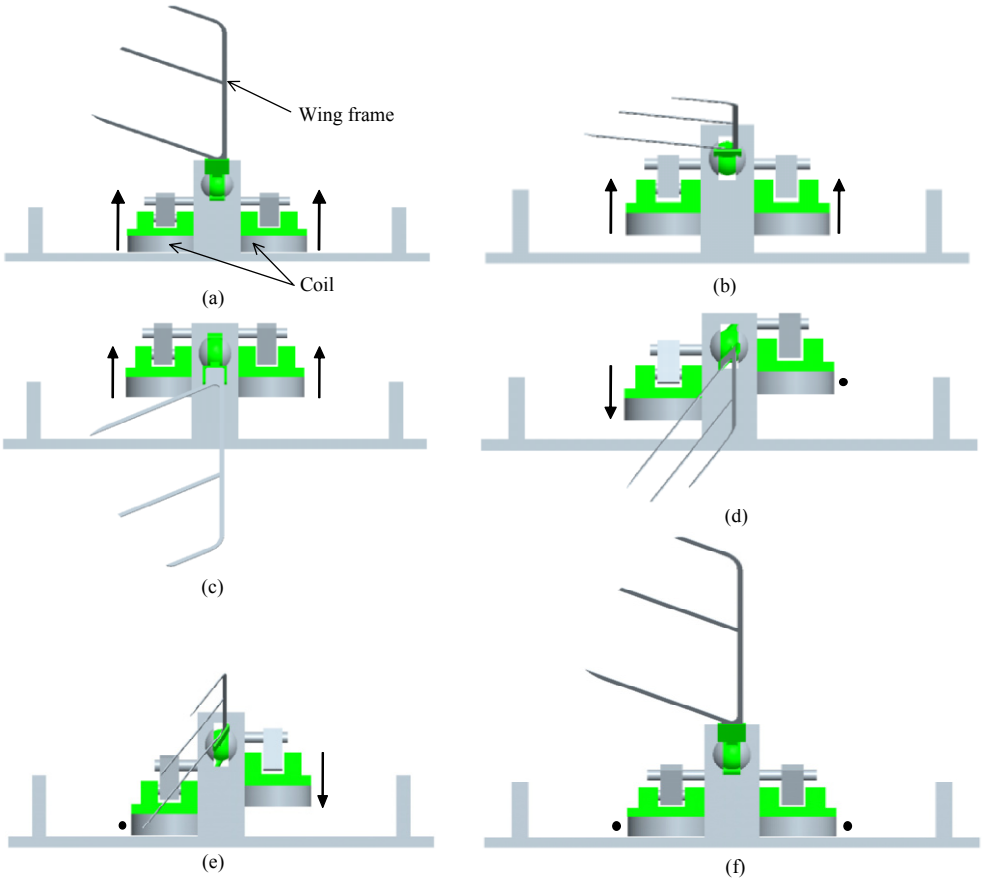

Fig. 2 Procedure of twisting of wing, (a) initial position of downstroke; (b) downstroke; (c) finish of downstroke; (d) twist before upstroke; (e) upstroke; and (f) finish of upstroke.

The stroke of the wings is generated by a linkage mechanism using two actuators. The schematic for this motion is shown in Fig. 3. The relationship between the stroke of the wing and the movement of the actuator can be obtained as

$$e_y = \sqrt{L_2^2 - (e_x^2 - 2e_x L_1 \cos\theta_r + L_1^2 \cos^2\theta_r)} + L_1 \sin\theta_r, \quad (3)$$

where e_y is the vertical movement of the coil, e_x is the horizontal distance between the ball joint and the coil, θ_r is the stroke of the wing, and L_1 and L_2 are the length of each link. This motion is more efficient if a longer flapping stroke, θ_r, is acquired by a shorter actuator movement. The derivative of θ_r with respect to e_y reflects the efficiency of the movement. The relation is expressed as

$$\frac{d\theta_r}{de_y} = \left(\frac{e_y}{L_1} - \sin\theta_r\right)\left(\frac{1}{e_y \cos\theta_r - e_x \sin\theta_r}\right). \quad (4)$$

The above relationship shows that θ_r becomes larger as L_1 shortens and e_x lengthens, for the same movement of the actuator. Even though it is possible to obtain a longer stroke by shortening L_1, its length is limited by the producible size of each part. In addition, despite the advantages of a longer stroke provided by a longer e_x, the dimension of e_x should be as short as possible to minimize wing span.

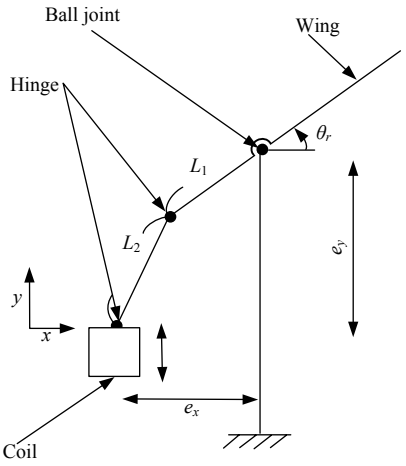

Fig. 3 Schematic of linkage for flapping motion.

3.2 The profile of input voltage for the twisting motion

In **3.1** a structural design for wing twisting while flapping was introduced. The input voltage of the flying robot should fulfill that both twisting and flapping motions can occur simultaneously. As shown in Fig. 2a, two coils move upwards at the same time during the downstroke. Then, the rear coil moves downwards while the front coil stays in place at the end of the downstroke to generate twisting motion. Finally, the front coil moves downwards while the rear coil stays in place at the end of the twisting motion to make the upstroke. The input voltage profile for each step of Fig. 2 is shown in Fig. 4. The duration, t_{twist}, represents the time needed to produce the twisting motion. Twist angle, θ_t, increases with t_{twist}. The full wing period, T, including the portion of the cycle where the coils are stationary, can be obtained as

$$T = T'(1 + \frac{\theta_t}{2\pi}), \tag{5}$$

by choosing proper T' and θ_t, where, T' indicates the desired period of the wing flapping.

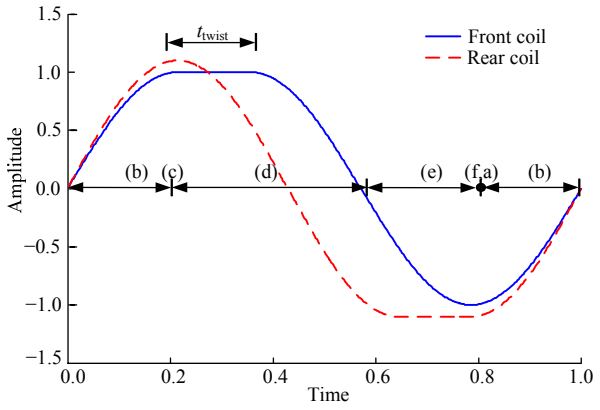

Fig. 4 Profile of input voltage to coil to generate flapping and twisting of wing.

3.3 Structure for low power consumption

The stroke of the wings is generated at a given frequency. If the exciting frequency is the same as the resonant frequency, the amount of power consumed for a given stroke can be reduced. The moving masses, such as the coil and the wing in Fig. 1, can be considered to be supported by springs. Therefore, the structure can be considered as a second order system with the masses of coil (m_c) and wing (m_w), and stiffness (k). Therefore, the resonant frequency, ω_n, is expressed as

$$m_c e_x^2 \ddot{\theta}_r + J_w \ddot{\theta}_r + k e_x^2 \theta_r = F_0 e_x$$
$$\rightarrow \omega_n = \sqrt{\frac{k e_x^2}{m_c e_x^2 + J_w}}, \tag{6}$$

where J_w is the mass moment of inertia of wing, which is obtained from CAD software. From Eq. (6), the resonant frequency gets larger as the stiffness of the spring gets larger, and the mass of the coil and the mass moment of inertia of the wing get smaller.

The stiffness of the spring should be selected to achieve the desired resonant frequency. The spring in Fig. 1 could be considered as a beam fixed on both ends. However, one end can only be moved in the direction of the upstroke/downstroke. Therefore, the stiffness of the beam, k, is expressed as[14]

$$F = \frac{12EI}{L^3} y \rightarrow k = \frac{12EI}{L^3}, \tag{7}$$

where y is the deflection with respect to x, E is Young's modulus and I is the moment of inertia. Here, the cross section of the spring is rectangular. Even though the mass and mass moment of inertia of moving parts, such as the coil and wings, are limited by design, the stiffness of the spring can be adjusted according to Eq. (7) to acquire the desired resonant frequency. In other words, the stiffness of the spring gets larger as the length of the spring (L) gets smaller, as well as when the width and height of the spring get larger.

In this work, the spring is made of stainless steel and is coated with tin for soldering wires to supply voltage to the coils.

3.4 Wing actuator

In this design, a VCM supported by springs is developed because it can be made compactly by eliminating the need for additional mechanical parts to transform rotary motion into linear motion. The developed actuator is composed of a solenoid coil (copper), a bobbin to support the coil (PEEK), and a permanent magnet (NeFeB). The magnetic force along upstroke/downstroke was estimated using FEM (MAXWELL V.10). The magnetic field for the case where the distance between the magnet and the coil is 1.0 mm is shown in Fig. 5. A smaller inner diameter of the coil provides a larger magnetic force because the magnetic field is more

uniform and its direction is the same as the direction of coil movement. However, the size of the coil is limited by production capabilities. The position of the coil along upstroke/downstroke, as a function of the voltage, can be obtained by identifying equilibrium between the spring force and the magnetic force. The required voltage into the coil is summarized in Table 1.

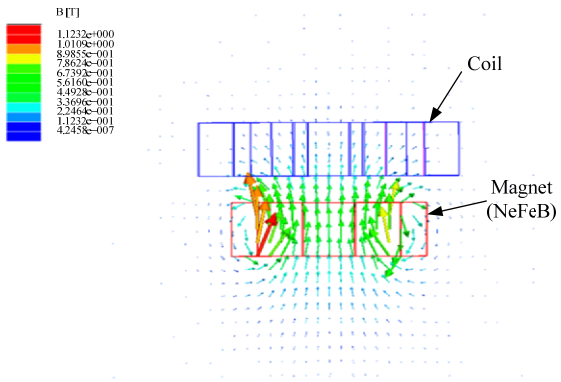

Fig. 5 Magnetic field produced by magnet and coil.

Table 1 Magnetic forces computed using FEM and spring forces obtained from Eq. (1)

Distance from magnet to solenoid (mm)	Magnetic force ($mN \cdot V^{-1}$)	Spring force (mN)	Required input voltage (V)
−1	372.8	593	−1.59
0	180.6	0	0
0.1	170.1	59.2	0.35
1	100.8	593	5.88

The resistance of each coil is about 25 Ω and the current into each coil is about 260 mA. In this design, an external battery is used to supply the driving power. If the vehicle were loaded with a 1.5 V/15 mAh mercury battery, which weighs 0.3 g, four batteries would be required to meet the required voltage, about 6 V as shown in Table 1. With the batteries, the flight time would last for about seven minutes.

3.5 Specifications based on flying insects

For hovering, wing area and flapping frequency are specified by Eq. (1), which shows that it is more advantageous for the flying robot to hover if it has a larger wing area and a faster flapping frequency. However, the primary design objective was to minimize the size of the robot. Therefore, the wing length must be short and the flapping frequency must be fast. Adequate wing lengths and flapping frequencies can be determined by investigating the mechanical characteristics of flying insects, such as the aspect ratio according to the mass, as well as the flapping or beating frequency according to the wing length[10]. The aspect ratio, AR, is defined as [10]

$$AR = \frac{L_{ws}^{\ 2}}{A}, \tag{8}$$

where the wing span L_{ws} is the length between the wing tips, A is the wing area. The design target for the aspect ratio is about 6 because the total mass of the flying robot is expected to be less than 3 g[10]. The design target for wing length is about 30 mm (L_{ws} = 60 mm) if the flapping frequency is selected as 60 Hz[10]. Thus, the needed wing area is 600 mm^2 by Eq. (8).

In this work, the veins of the wings were made of 0.1 mm diameter stainless steel. The wing membrane was made of 10 μm thickness polyurethane film.

4 Results and discussion

The components of the flapping-wing air vehicle were assembled as shown in Fig. 6. The total mass of the robot was 2.86 g, the wing span was 75 mm and the ratio of wing mass to body mass was 2.5%. The mass of each component is summarized in Table 2.

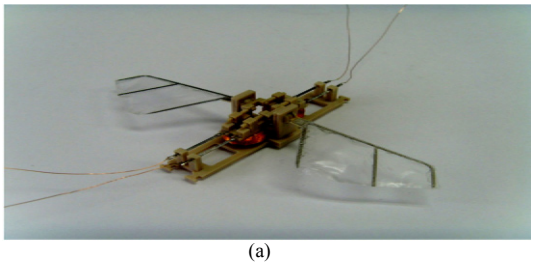

(a)

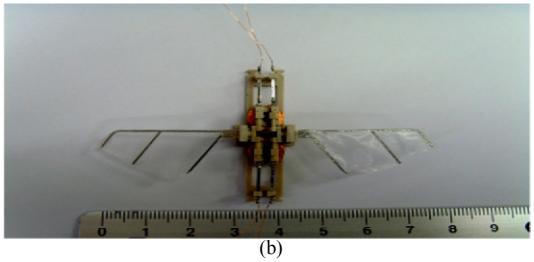

(b)

Fig. 6 Assembled air vehicle, (a) perspective view, and (b) top view.

Table 2 Masses of components of the air vehicle

Component	Mass (g)
Actuator	1.09
Magnet	0.83
Body frame	0.71
Wings (×2)	0.07
Others	0.16
Total	2.86

The resonant frequencies of the actuator and the system including the wings were 163 Hz and 62 Hz, respectively. Theses values were obtained analytically from Eq. (6) and Eq. (7). The experimentally determined resonant frequencies were 165 Hz and 68 Hz, respectively, as shown in Fig. 7. The properties of plate spring and wing used in the experiment are summarized in Table 3. Fig. 7b shows the first resonant frequency measured at the wing root of the assembled flapping-wing air vehicle. From Fig. 7a, the DC sensitivity of the resultant static force was 0.26 mm·V^{-1} when measured at a low frequency (10 Hz). Based on the simulation of the magnetic force the sensitivity was predicted to be 0.29 mm·V^{-1}.

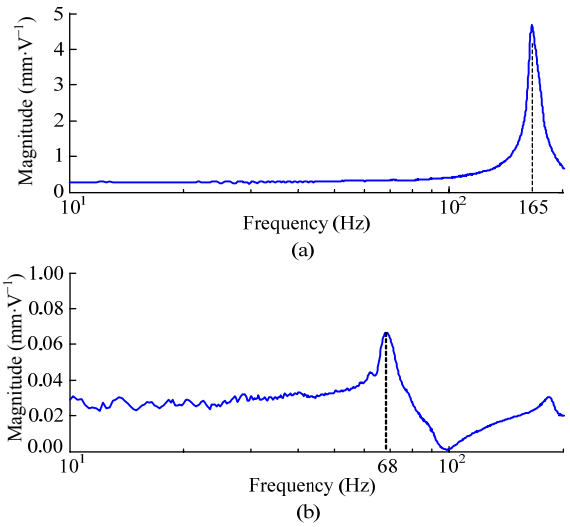

Fig. 7 Frequency response characteristics of (a) an actuator, and (b) the wing root of the air vehicle.

Table 3 Properties of plate spring and wing

Plate spring	
W(mm) × H(mm) × L(mm)	0.8×0.3×9
Young's Modulus (GPa)	10
Wing	
Mass moment of inertia (kg·m^2)	7.32×10^{-8}
Length (mm)	27

The vertical force as a function of twist angle, at the resonant frequency of the system (68 Hz) was measured by a load cell (Bongshin Loadcell, OBU Type 100 gf, http://www.loadcell.co.kr) as shown in Fig. 8a. The performance of the load cell as a function of its weight is shown in Fig. 8b. The data were obtained through five experiments as shown in Table 4. The load cell generates a negative voltage when a weight is applied downward, corresponding to a negative weight. The weight to voltage relation for the load cell is linear. The linearity is reliable because the maximal standard deviation is less than 0.0033 V as shown in Table 4.The motion of the wing generated by the movement of the actuators was captured by high speed camera (Fig. 9). From the high speed camera footage, the angles between the leading and the trailing edge of wings were measured, which was considered as the twist angle. The measured twist angles and their standard deviations are shown in Fig. 10. The twist angle trajectories are reasonably consistent during repeated experiments. The maximal standard deviation is 5.7°. The twist angle during the downstroke changed according to the expected input twist angle. However, the magnitude of this change had a similar trend according to the expected input twist angle. The twist angle during the upstroke increased although it was saturated at about 24° from the expected input twist angle of 60° due to the friction of the sliding guider (Fig. 1) caused by the arc movement of the actuator. Overall, an average positive lift was generated. Lift as a function of expected input twist angle is summarized in Fig. 11. Standard deviation bars are illustrated together. Fig. 11 demonstrates that lift increases linearly as expected input twist angle increases up to 60°.

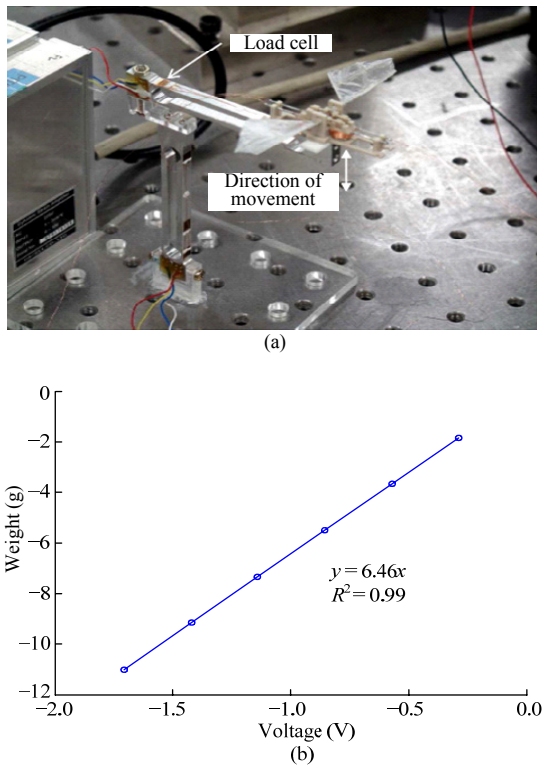

Fig. 8 (a) Load cell to measure the lifting force, and (b) its weight to voltage curve.

Table 4 Data for weight to voltage curve

Weight (g)	Voltage (V)						Standard deviation
	#1	#2	#3	#4	#5	Average	
−1.84	−0.286	−0.287	−0.286	−0.286	−0.287	−0.286	0.0005
−3.67	−0.572	−0.571	−0.576	−0.574	−0.574	−0.573	0.0019
−5.50	−0.856	−0.854	−0.856	−0.857	−0.858	−0.856	0.0015
−7.35	−1.138	−1.140	−1.139	−1.138	−1.139	−1.139	0.0008
−9.16	−1.416	−1.419	−1.416	−1.416	−1.417	−1.417	0.0013
−11.01	−1.698	−1.706	−1.698	−1.699	−1.700	−1.700	0.0033

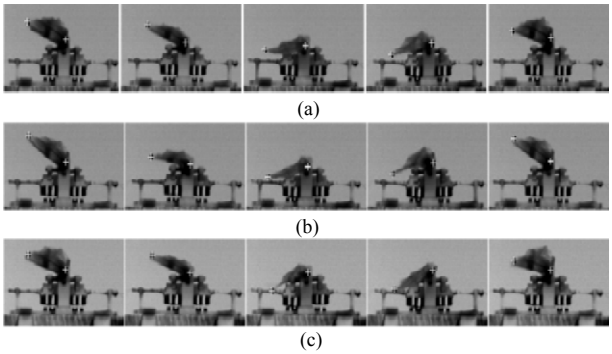

Fig. 9 Twisting motions, captured by a high speed camera, with flapping frequency of 68 Hz, (a) at $\theta_t = 0^\circ$; (b) at $\theta_t = 30^\circ$; and (c) at $\theta_t = 150^\circ$.

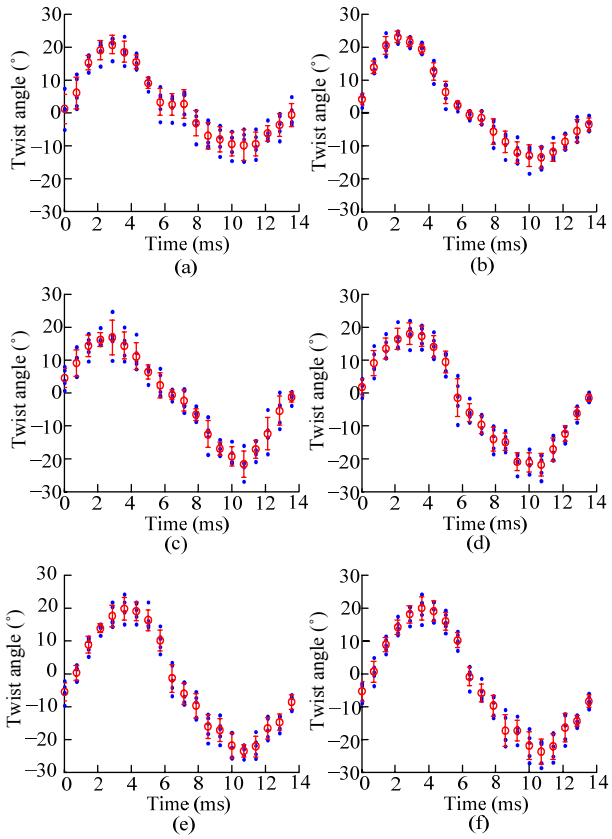

Fig. 10 Measured twist angle profiles with flapping frequency of 68 Hz, (a) at $\theta_t = 0^\circ$; (b) at $\theta_t = 30^\circ$; (c) at $\theta_t = 60^\circ$; (d) at $\theta_t = 90^\circ$; (e) at $\theta_t = 120^\circ$; and (f) at $\theta_t = 150^\circ$.

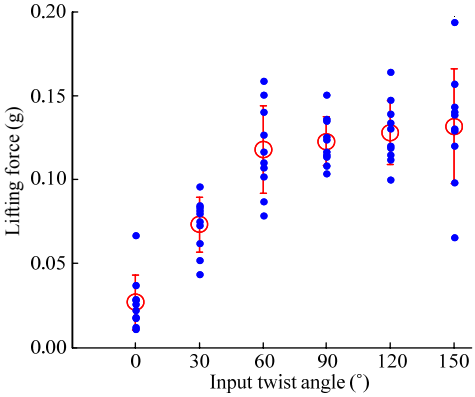

Fig. 11 Resultant lifting forces over twist angles. The measured lifting forces are represented by "●", the average lifting forces by "○" and the standard deviation of lifting force by bar.

Normalized vertical force profiles over a wing cycle period are shown in Fig. 12. The vertical forces are normalized by the maximum and minimum experimental values. The normalizing factors were fixed with the case of the twist angle at $\theta_t = 0^\circ$ (no twisting motion) for the others. Each graph shows both the normalized vertical forces obtained by experiment and by computation from two theoretical models (Eq. (1)), one of which takes into account the twist angle change over time and the other does not. The twist angle change is reflected to the change of the effective area of wing over time. This enables the investigation of the effect of twist angle on vertical force. The results demonstrate that the effective wing area is decreased by the proposed mechanism because the experimentally obtained vertical force values were closer to the values predicted by the theoretical model that included the twist angle than to the values predicted by the model that did not include it.

5 Conclusion

We proposed a mechanism to actively twist robotic wings while flapping them by using two VCMs. By capturing the flapping and twisting motions according to the expected input twist angle, the actual twist angle was acquired. The assembled flapping-wing air vehicle, which weighed 2.86 g, produced an average positive vertical force that was proportional to the twist angle. The force saturated because the twisting angle was mechanically limited. In future studies, new designs will be considered to obtain true linear motion of the actuator during the stroke and to sustain the expected twist angle by using stiffer materials at the wing root. These design changes will enable us to achieve a larger twist angle

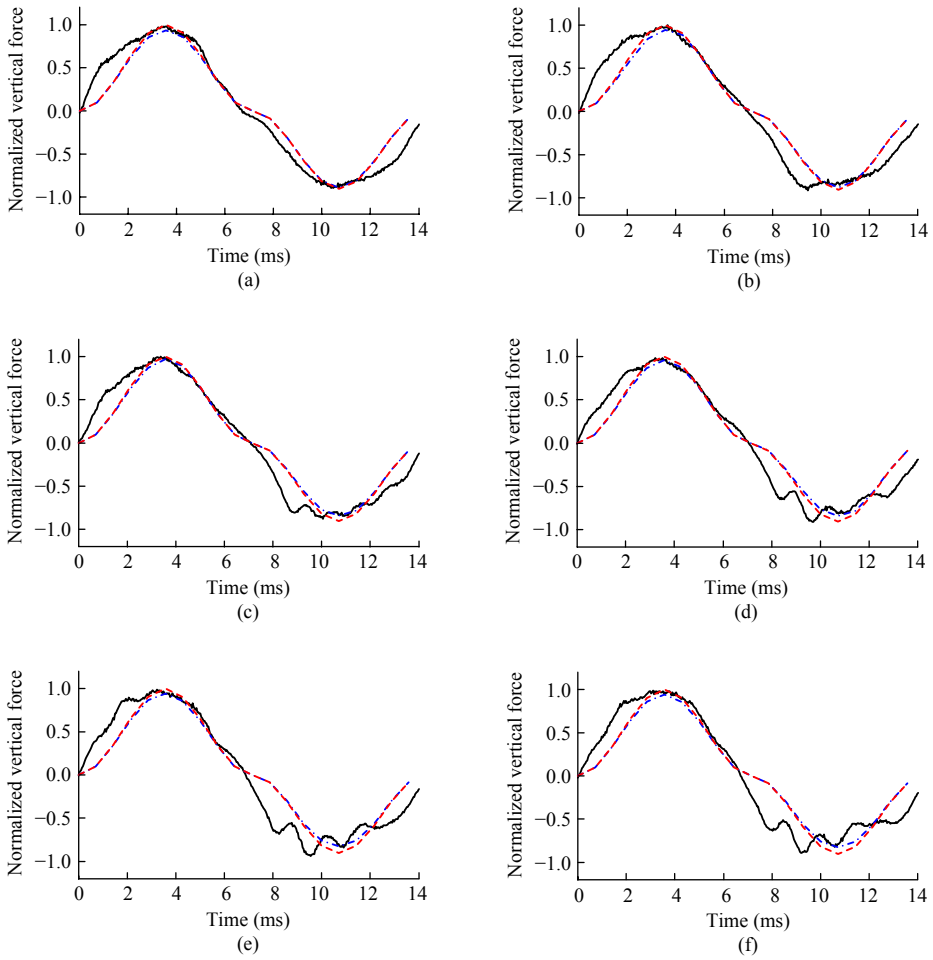

Fig. 12 Normalized vertical force profiles with flapping frequency of 68 Hz, (a) at $\theta_t = 0^\circ$, (b) at $\theta_t = 30^\circ$, (c) at $\theta_t = 60^\circ$, (d) at $\theta_t = 90^\circ$, (e) at $\theta_t = 120^\circ$, and (f) at $\theta_t = 150^\circ$. "–" represents the profiles measured by the load cell. "– · –" and "- - -" show the profiles computed by the theoretical models with and without considering the twist angle changes over time, respectively.

that will produce greater lift. To enhance the performance, further study on the design of the wing structure is also required[15,16].

Acknowledgment

This work was supported by Korea government, Ministry of Knowledge Economy under Human Resources Development Program for Convergence Robot Specialists and Ministry of Education, Science and Technology under KRF grant (No. 2010-0015226).

References

[1] Nguyen Q V, Park H C, Goo N S, Byun D Y. Characteristics of a beetles free flight and a flapping-wing system that mimics beetle flight. *Journal of Bionic Engineering*, 2010, **7**, 77–86.

[2] Fujikawa T, Sato Y, Makata Y, Yamashita T, Kikuchi K. Motion analysis of butterfly-style flapping robot for different wing and body design. *Proceedings of IEEE International Conference on Robotics and Biomimetics* (*ROBIO* 2008), Bangkok, 2009, 216–221.

[3] Wood R J. The first takeoff of a biologically inspired at-scale robotic insect. *IEEE Transactions on Robotics*, 2008, **24**, 341–347.

[4] Sitti M. Piezoelectrically actuated four-bar mechanism with two flexible links for micromechanical flying insect thorax. *IEEE/ASME Transactions on Mechatronics*, 2003, **8**, 26–36.

[5] Żbikowski R, Galiński C, Pedersen C B. Four-bar linkage mechanism for insectlike flapping wings in hover. *Journal of Mechanical Design*, 2005, **127**, 817–824.

[6] McIntosh S H, Agrawal S K, Khan Z. Design of a mechanism for biaxial rotation of a wing for a hovering vehicle. *IEEE/ASME Transactions on Mechatronics*, 2006, **11**, 145–153.

[7] Norberg R Å. The pterostigma of insect wings an inertial regulator of wing pitch. *Journal of Comparative Physiology*

A, 1972, **81**, 9–22.

[8] Dudley R. *The Biomechanics of Insect Flight*: *Form*, *Function and Evolution*, Princeton University Press, Princeton, USA, 2000.

[9] Ellington C P. The aerodynamics of hovering insect flight. II. Morphological parameters. *Philosophical Transactions of the Royal Society of London B*, 1984, **305**, 17–40.

[10] Azuma A. *The Biokinetics of Flying and Swimming*, American Institute of Aeronautics and Astronautics, Inc., El Segundo, USA, 2006.

[11] Betts C. The comparative morphology of the wings and axillae of selected heteroptera. *Journal of Zoology*, 1986, **1**, 255–282.

[12] Ennos A. The effect of size on the optimal shapes of gliding insects and seeds. *Journal of Zoology*, 1989, **219**, 61–69.

[13] Dudley R. Biomechanics of flight in neotropical butterflies: Morphometrics and kinematics. *Journal of Experimental Biology*, 1990, **150**, 37–53.

[14] Hibbeler R. *Mechanics of Materials*, 2nd edition, Macmillan College Publishing Company, New York, USA, 1994.

[15] Jongerius S, Lentink D. Structural analysis of a dragonfly wing. *Experimental Mechanics*, 2010, **50**, 1323–1334.

[16] Wootton R J, Herbert R C, Young P G, Evans K E. Approaches to the structural modelling of insect wings. *Philosophical Transactions of the Royal Society of London B*, 2003, **358**, 1577–1587.